Journal Name

COMMUNICATION

N and S co-doped porous carbon spheres prepared using L-cysteine as a dual function agent for high-performance lithium-sulfur batteries

Received 00th January 20xx,
Accepted 00th January 20xx

DOI: 10.1039/x0xx00000x

www.rsc.org/

Shuzhang Niu,‡[a,b] Wei Lv,‡[a] Guangmin Zhou,[c] Yanbing He,[a] Baohua Li,[a] Quan-Hong Yang,[a,d*] Feiyu Kang[a,b*]

Nitrogen and sulfur co-doped porous carbon spheres (NS-PCSs) were prepared using L-cysteine to control the structure and the functionalization during the hydrothermal reaction of glucose and the following activation process. As the sulfur hosts in Li-S batteries, NS-PCS combine strong physical confinement and surface chemistry interaction to improve the affinity of polysulfides to carbon matrix.

The lithium-sulfur battery has attracted significant attention due to its high specific energy density (2600 Wh kg^{-1}), non-toxicity and the abundance of sulfur in nature.[1] However, there are two drawbacks to using sulfur: its low utilization due to its inferior electronic conductivity, and a rapid capacity fade resulting from the high dissolution of the soluble intermediates during the charge-discharge process. An effective strategy to solve these problems is to select specific carbon materials as hosts for the sulfur, such as graphene,[2, 3] carbon nanotubes,[4] porous carbons fibres,[5] and porous carbon,[6, 7] to increase the utilization of active material and alleviate the dissolution of polysulfides into the electrolyte. Carbons with a large surface area and a hierarchical pore structure are therefore preferred. Additionally, several studies have shown that doping carbon materials with heteroatoms (nitrogen, boron, sulfur and phosphorous) is a promising way to further improve the electric conductivity and electrochemical activity.[8] N-doped carbons have been proved to promote the interaction of sulfur atoms with the carbon matrix.[9] Sulfur doping can also enhance the affinity of polysulfides to the carbons with better cycling behaviour.[10, 11] Zhou *et al*.[12] presented a Li/polysulphide battery with a high-energy density and long-cyclic life using three-dimensional nitrogen/sulphur co-doped graphene sponge electrodes. Thus, it is vital to design a novel carbon material, which not only possesses a high specific surface area (SSA) and a hierarchical pore structure to obtain a high loading of sulfur and facilitate fast Li ion and electron transport, but also has a specific surface chemistry to increase the affinity between the polysulfides and the carbon matrix. However, in most cases, the structure control and functionalization are two separate processes which result in a complex preparation method. Moreover, functionalization after the formation of a complex pore structure may not be uniform and always results in a low doping level.

Here, we propose a simple yet effective strategy to turn glucose-derived carbon spheres with a microporous structure into heteroatom-doped porous carbon spheres with a hierarchical pore structure by introducing an agent in the preparation process that serves two functions. More interestingly, the doped carbons have much larger size than the undoped ones. Typically, N and S co-doped porous carbon spheres (NS-PCSs) are prepared through a simple hydrothermal treatment of D-glucose and L-cysteine and later KOH activation. The L-cysteine not only acts as a functionalization agent to provide the source for N and S doping, but also as a pore structure modifying agent to turn the microporous structure into a hierarchical pore structure. The NS-PCSs obtained have a high specific surface area (SSA) of 2583 m^2 g^{-1}, a large pore volume (2.6 cm^3 g^{-1}) and a broader pore size distribution, from micropores to mesopores, which provide space for high sulfur loading. They also accommodate the volume expansion of sulfur during charge-discharge process and facilitate fast Li ion diffusion. In addition, the *in-situ* N and S co-doping guarantees the uniform distribution of the doping elements and further increases the affinity of polysulfides to the carbon surface (Fig. S1, ESI†). As a result of the synergistic effect of pore structure and surface functionalization, the prepared NS-PCS/sulfur (NS-PCS/S) hybrid exhibits a high capacity, an excellent rate capability as well as a stable cycling performance.

The preparation process of the NS-PCS is illustrated in Fig. 1a. D-glucose as a carbon source was first dissolved in deionized water to form a homogeneous solution and then L-cysteine, as a source of both nitrogen and sulfur, was added under stirring to this solution with a L-cysteine/glucose weight ratio of 1:5. The uniformly mixed solution was filled into a Teflon liner where it underwent hydrothermal treatment, and the obtained carbon spheres were collected, washed and dried. Finally, the carbon spheres went through a KOH activation process to obtain the NS-PCSs. For comparison, porous carbon spheres (PCSs) were also prepared under the same conditions but without L-cysteine. The NS-PCSs and the

[a.] Engineering Laboratory for Functionalized Carbon Materials and Shenzhen Key Laboratory for Graphene-based Materials, Graduate School at Shenzhen, Tsinghua University, Shenzhen 518055, China.
Email: yang.quanhong@sz.tsinghua.edu.cn; fykang@sz.tsinghua.edu.cn
[b.] School of Materials Science and Engineering, Tsinghua University, Beijing 100084, China.
[c.] Shenyang National Laboratory for Materials Science, Institute of Metal Research, Chinese Academy of Sciences, Shenyang 110016, China
[d.] School of Chemical Engineering and Technology, Tianjin University, Tianjin 300072, China. Email: qhyangcn@tju.edu.cn (Q. H. Yang).

†Electronic Supplementary Information (ESI) available: Details of the sample preparation and characterization results of the NS-PCS/S hybrid and other reference samples. See DOI: 10.1039/x0xx00000x

‡These two authors are equal main contributions.

PCSs were infiltrated with S using a melt-infusion method to obtain NS-PCS/S and PCS/S hybrids. The detailed preparation process is provided in the Supporting Information.

The structures of the PCSs and NS-PCSs were investigated by scanning (SEM) and transmission electron microscopy (TEM). As shown in Fig. 1b, the PCSs have a spherical shape and a certain degree of agglomeration. When adding the L-cysteine as nitrogen and sulfur source, the NS-PCSs still have a uniform spherical shape with a size range of 5-8 μm and a rough surface (Fig. 1c). From a comparison of the NS-PCSs and PCSs, we can see that the NS-PCSs have a much larger particle size than PCSs, indicating that the addition of L-cysteine affects the growth of the carbon spheres in the hydrothermal process, which is mainly attributed to Maillard type reactions. While both amines and thiols of the L-cysteine can react with the aldehyde group of the glucose molecule and give rise to a variety of products which result in the early formation of nucleation seeded larger size.[13, 14] The detailed process is being investigated. A high-resolution TEM image shows their amorphous nature (Fig. 1d and e), but no obvious differences between them can be observed.

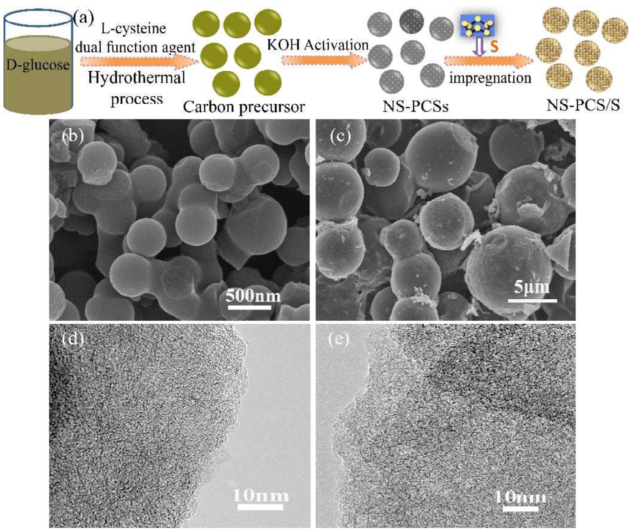

Fig. 1 (a) Schematic of the synthesis of NS-PCSs and the NS-PCS/S hybrid. SEM images of (b) PCSs and (c) NS-PCSs. TEM images of (d) a PCS and (e) a NS-PCS.

The structural difference between PCSs and NS-PCSs can be well reflected by the N_2 adsorption-desorption isotherms. The isotherm of NC-PCSs shows combined characteristics of type I and IV isotherms according to the IUPAC classification (Fig. 2a), which indicates the presence of a broad pore size distribution ranging from micropores to mesopores. From the pore size distribution (PSD) result (Fig. 2a, inset), besides micro-pores of around 0.8 nm and 1.2 nm diameter, mesopores of diameter 3-6 nm exist forming a hierarchical pore structure, which is beneficial for restricting the dissolution of polysulfides and facilitating the fast migration of Li ions. The specific surface area and pore volume of NS-PCSs are about 2583 $m^2\ g^{-1}$ and 2.6 $cm^3\ g^{-1}$, respectively, which are much higher than the values for PCS (2157 $m^2\ g^{-1}$ and 1.17 $cm^3\ g^{-1}$) and reported porous carbon spheres.[15, 16] The PCSs mainly shows a type I isotherm indicating its microporous structure which is consistent with the PSD result shown in Fig. 2a. These results clear show the L-cysteine not only affects the formation process of the carbon spheres but also acts as a pore modifying agent, possibly due to its ultralow charring yield in the activation process leaving abundant pores. Raman spectra further show the structural differences of NS-PCSs and PCSs. In Fig. 2b, the two samples show two evident peaks around 1348 and 1594 cm^{-1}, which correspond to the D and G bands, respectively.[17] The intensity ratios (I_D/I_G) for PCSs and NS-PCSs are 1.04 and 1.15, respectively. The increased value for NS-PCSs is possibly caused by defects in the carbon framework and heteroatom doping.[18, 19]

Heteroatom doping caused by the L-cysteine was further elucidated by X-ray photoelectron spectroscopy (XPS). The XPS survey spectrum of NS-PCSs (Fig. S2a, ESI †) shows four characteristic peaks at around 164, 285, 399 and 532 eV, corresponding to the S2p, C1s, N 1s and O1s, respectively. The elemental contents of N and S in NS-PCSs are 2.05 wt% and 0.56 wt%, respectively. In addition, the element analysis shows the nitrogen and sulfur content in the NS-PCS are about 2.85 wt% and 0.95 wt%, which is in accordance with the XPS results, indicating the uniform distribution of N and S elements in bulk particles. For PCSs, no N and S signals can be detected (Fig. S2b, ESI†). High-resolution C1s spectra of NS-PCSs (Fig. S3b, ESI†) can be divided into several peaks corresponding to C-C (284.5 eV), C=N/C-OH (285 eV), C=O (285.6 eV), O-C=O (289.1 eV), C-S (283.8 eV) and C-N (287 eV), which is different from PCSs (Fig. S3a, ESI†).[20] As shown in Fig. 2c, the N1s spectrum is divided into three typical peaks located at 398.4, 400.1 and 401.2 eV, which are attributed to pyridinic, pyrrolic and graphitic nitrogen, respectively.[21] The existence of pyridinic-N and pyrrolic-N helps improve the electrochemical activity.[22] Meanwhile, nitrogen doping in the carbon material can effectively increase chemical adsorption between sulfur atoms and functional groups on the carbon.[23] In the S2p spectrum of the NS-PCSs (Fig. 2d), the peaks at 163.8 and 165.0 eV represent S atoms connected to carbon atoms, and the peak at 168.8 eV belongs to oxidized S (SO_x). Doping S in the NS-PCSs can positively modify the catalytic properties as reported for some S-doped materials.[24, 25]

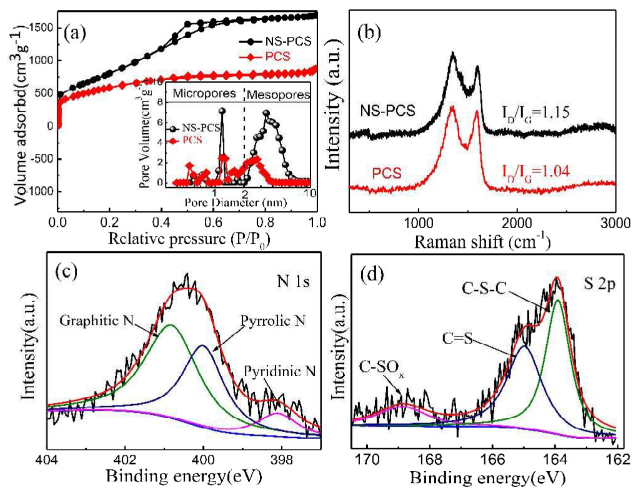

Fig. 2 (a) Nitrogen adsorption-desorption isotherms and pore-size distributions (insets) of the NS-PCSs and PCSs. (b) Raman spectra of the NS-PCSs and PCSs. High-resolution (c) N1s and (d) S2p XPS spectra of the NS-PCSs.

To have a sulfur/carbon electrode for Li-S battery, sulfur is infiltrated into the NS-PCSs matrix by a melt-diffusion method. The SSA of the NS-PCS/S hybrid is reduced to 260.2 $m^2\ g^{-1}$ and some micropores and small mesopores still exist (Fig. S4, ESI†), which facilitate the ion diffusion in electrochemical reactions. These results also indicate that some sulfur are not immersed into the pores, which can be further proved by the TG results discussed later. The sulfur content of this hybrid is about 64.5 wt%, which is demonstrated by TG-DSC curves (Fig. S5a, ESI†). For the TG curves of NS-PCS/S hybrid, it shows two weight loss at around 160 ^oC and 260 ^oC, which can be attributed to the loss of the sulfur situated at the outer surface and confined in the pores of the carbon spheres, respectively.[26] The sulfur at the surface contributes the strong diffraction peaks in the XRD patterns (Fig. S6, ESI†). In addition, sulfur in the pores of NS-

PCSs and PCSs shows higher thermal stability than pure sulfur due to the strong capillary force (Fig. S5, ESI†).[27] STEM images of the NS-PCS/S hybrid and the corresponding carbon and sulfur (Fig. S7, ESI†) elemental maps also show that sulfur has uniformly dispersed in the NS-PCS framework. The linear analysis (Fig. S8, ESI†) along the diameter of the NS-PCS/S hybrid further proves the uniform distribution of the sulfur in the sphere.

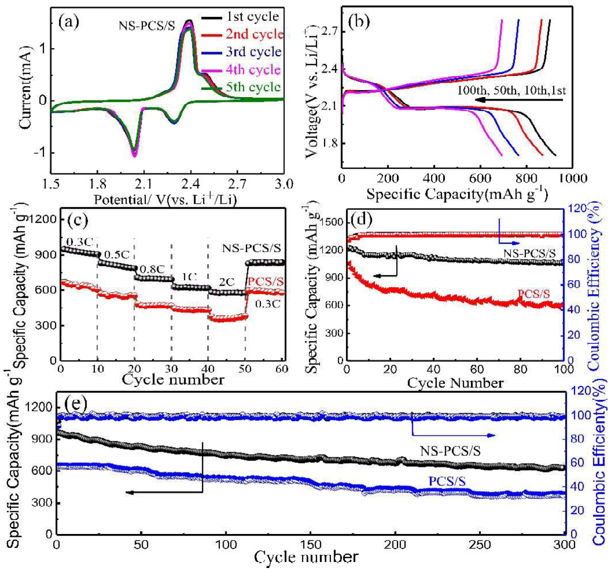

Fig. 3 (a) CV curves and (b) discharge-charge voltage profiles of the NS-PCS/S hybrid at 0.3C. (c) Discharge capacities at different current rates and the cycle performance of the NS-PCS/S and PCS/S hybrids at (d) 0.1 C and (e) 0.3C.

Coin cells (2032) using metallic lithium as the anode and the NC-PCS/S hybrid as the cathode were assembled to evaluate the electrochemical performances. For comparison, the performance of the PCS/S hybrid (with similar sulfur content, Fig. S5b, ESI†) was also investigated under the same conditions. Fig. 3a presents the CV curves of the NS-PCS/S electrode with a scan rate of 0.1mV s^{-1}. Two main cathodic peaks at about 2.30 V and 2.05 V in the first cycle are attributed to the change of sulfur to higher-order lithium polysulfide (Li_2S_n, $3 \leq n \leq 8$) and the further reduction of high-order lithium polysulfides to Li_2S_2 and eventually to Li_2S, respectively.[28] Two oxidation reaction peaks are observed in the NS-PCS/S electrode, the first peak at 2.38 V is associated with the formation of Li_2S_n ($3 \leq n \leq 8$) and the second peak at 2.48 V corresponds to the formation of elemental sulfur.[29] The CV curves are almost overlapping for the first five cycles, suggesting high reversibility, which is superior to that shown by PCS/S hybrid (Fig. S9, ESI†). The discharge-charge voltage profile (Fig. 3b) displays a high initial discharge capacity of ~938 mAh g^{-1} (based on the mass of S) at 0.3C (1C=1675 mA g^{-1}). In contrast, the capacity of the PCS/S hybrid is only 675 mAh g^{-1} (Fig. 3c). Moreover, two typical discharge plateaus at around 2.3V and 2.05V are observed, which correspond to the two reduction peaks in Fig. 3a. After 100 cycles, the plateaus still exist, indicating good stability. Fig. 3c shows the rate performance of the NS-PCS/S and PCS/S hybrids, with the former showing a much better performance. Fig. 3d gives the cycling performance of the NS-PCS/S and PCS/S hybrids at a rate of 0.1C. The NS-PCS/S delivers a high specific capacity of 1265 mAh g^{-1} in the initial cycle and 1032 mAh g^{-1} after 100 cycles. In contrast, the capacity of PCS/S dropped from 1100 to 605 mAh g^{-1}. A prolonged cycling test was also conducted for NS-PCS/S and PCS/S hybrids at 0.3C (Fig. 3e), an initial discharge capacity of 942 mAh g^{-1} was delivered and the reversible capacity still remained 629 mAh g^{-1} after 300 cycles with only 0.11% capacity fade per cycle, which is higher than the PCS/S hybrid (335 mAh g^{-1}). In addition, we also prepared the nitrogen doped porous carbon spheres (N-PCSs) as sulfur host, which shows relatively inferior electrochemical performance than NS-PCS/S hybrid (Fig. S10, ESI†), further testifying the N, S co-doping can further improve the performance of a C/S electrode compared to the N only-doped case.

Generally, the excellent electrochemical performance of NS-PCS/S can be ascribed to the synergistic effect of a hierarchical pore structure and N and S co-doping. On the one hand, the hierarchical pore structure of the NS-PCSs not only provides a large space for high sulfur loading, but also effectively traps the intermediate polysulfide and facilitates fast Li ion immigration. On the other hand, the N, S-codoping increases the conductivity and electrochemical activity of the NS-PCSs. More importantly, N and S codoping can further increase the chemical adsorption between sulfur atoms and oxygen functional groups on the carbon framework, and thus improve the cyclic stability. The EIS measurement further supports the above points (Fig. S11, ESI†). The semicircle in the high frequency region corresponds to the charge-transfer resistance (R_{ct}) occurring at the electrolyte-electrode interface and the straight line in the low frequency region corresponds to a semi-infinite Warburg diffusion process.[30] Before discharge, the charge-transfer resistance (R_{ct}) of NS-PCS/S is 28.1Ω while this value for PCS/S is 39.4Ω, which can be attributed to the increased conductivity and electrochemical activity originating from the N and S doping and the strong interaction between the heteroatoms and the sulfur.

In summary, N and S co-doped porous carbon microspheres with a large SSA and a hierarchical pore structure were prepared by using a chemical, L-cysteine that serves as two functions. It not only acts as the heteroatom doping source but also a pore modifying agent. Due to the synergistic effect of the hierarchical pore structure and the N and S co-doping, the NS-PCS/S hybrid cathode delivers a high initial capacity of 942 mAh g^{-1} and maintains a reversible capacity of 629 mAh g^{-1} after 300 cycles at 0.3C with only 0.11% capacity fade per cycle. This work not only provides a new carbon material for use in high performance lithium-sulfur batteries, but also presents an effective strategy to simultaneously tune the structure and surface chemistry of carbon materials by selecting and introducing suitable multi-functional agents although the detailed process are awaiting a detailed investigation.

This work was supported by the National Basic Research Program of China (2014CB932400), National Natural Science Foundation of China (Nos. 51372167, 51302146 and U1401243) and Shenzhen Basic Research Project (No. ZDSYS20140509172959981). We also appreciate financial support from the Guangdong Province Innovation R&D Team Plan (No. 2009010025).

Notes and references

1. A. Manthiram, Y. Fu, S.-H. Chung, C. Zu and Y.-S. Su, *Chem. Rev.*, 2014, **114**, 11751-11787.
2. C. Zhang, W. Lv, W. Zhang, X. Zheng, M.-B. Wu, W. Wei, Y. Tao, Z. Li and Q.-H. Yang, *Advanced Energy Materials*, 2014, **4**, 1301565.
3. W. Lv, Z. Li, G. Zhou, J.-J. Shao, D. Kong, X. Zheng, B. Li, F. Li, F. Kang and Q.-H. Yang, *Advanced Functional Materials*, 2014, **24**, 3456-3463.
4. L. Wang, Y. Zhao, M. L. Thomas and H. R. Byon, *Advanced Functional Materials*, 2014, **24**, 2248-2252.
5. L. Miao, W. Wang, K. Yuan, Y. Yang and A. Wang, *Chemical Communications*, 2014, **50**, 13231-13234.
6. W. Hu, H. Zhang, Y. Zhang, M. Wang, C. Qu and J. Yi, *Chemical Communications*, 2015, **51**, 1085-1088.

7. S. Niu, W. Lv, C. Zhang, F. Li, L. Tang, Y. He, B. Li, Q.-H. Yang and F. Kang, *Journal of Materials Chemistry A*, 2015, DOI: 10.1039/C5TA05324B.
8. J. P. Paraknowitsch and A. Thomas, *Energy & Environmental Science*, 2013, **6**, 2839-2855.
9. H.-J. Peng and Q. Zhang, *Angewandte Chemie International Edition*, 2015, **54**, 11018-11020.
10. K. A. See, Y.-S. Jun, J. A. Gerbec, J. K. Sprafke, F. Wudl, G. D. Stucky and R. Seshadri, *Acs Appl Mater Inter*, 2014, **6**, 10908-10916.
11. Z. Yang, Y. Dai, S. Wang, H. Cheng and J. Yu, *RSC Adv.*, 2015, **5**, 78017-78025.
12. G. Zhou, E. Paek, G. S. Hwang and A. Manthiram, *Nat Commun*, 2015, **6**, DOI:10.1038/ncomms8760.
13. C. Billaud, C. Maraschin, Y.-N. Chow, S. Chériot, M.-N. Peyrat-Maillard and J. Nicolas, *Molecular Nutrition & Food Research*, 2005, **49**, 656-662.
14. S. A. Wohlgemuth, F. Vilela, M. M. Titirici and M. Antonietti, *Green Chem.*, 2012, **14**, 741-749.
15. B. Zhang, X. Qin, G. R. Li and X. P. Gao, *Energy & Environmental Science*, 2010, **3**, 1531-1537.
16. W. Zhou, C. Wang, Q. Zhang, H. D. Abruña, Y. He, J. Wang, S. X. Mao and X. Xiao, *Advanced Energy Materials*, 2015, **5**, 1401752.
17. Q.-H. Yang, P.-X. Hou, M. Unno, S. Yamauchi, R. Saito and T. Kyotani, *Nano Lett*, 2005, **5**, 2465-2469.
18. W. Ai, Z. Luo, J. Jiang, J. Zhu, Z. Du, Z. Fan, L. Xie, H. Zhang, W. Huang and T. Yu, *Advanced Materials*, 2014, **26**, 6186-6192.
19. S. Niu, W. Lv, C. Zhang, Y. Shi, J. Zhao, B. Li, Q.-H. Yang and F. Kang, *Journal of Power Sources*, 2015, **295**, 182-189.
20. D. Sun, J. Yang and X. Yan, *Chemical Communications*, 2015, **51**, 2134-2137.
21. Y. Mao, H. Duan, B. Xu, L. Zhang, Y. Hu, C. Zhao, Z. Wang, L. Chen and Y. Yang, *Energy & Environmental Science*, 2012, **5**, 7950-7955.
22. F. Sun, J. Wang, H. Chen, W. Li, W. Qiao, D. Long and L. Ling, *Acs Appl Mater Inter*, 2013, **5**, 5630-5638.
23. J. Song, T. Xu, M. L. Gordin, P. Zhu, D. Lv, Y.-B. Jiang, Y. Chen, Y. Duan and D. Wang, *Advanced Functional Materials*, 2013, **24**, 1243-1250.
24. W. Kiciński, M. Szala and M. Bystrzejewski, *Carbon*, 2014, **68**, 1-32.
25. W. Gu, M. Sevilla, A. Magasinski, A. B. Fuertes and G. Yushin, *Energy & Environmental Science*, 2013, **6**, 2465-2476.
26. J. Kim, D.-J. Lee, H.-G. Jung, Y.-K. Sun, J. Hassoun and B. Scrosati, *Advanced Functional Materials*, 2013, **23**, 1076-1080.
27. C. Liang, N. J. Dudney and J. Y. Howe, *Chemistry of Materials*, 2009, **21**, 4724-4730.
28. N. Jayaprakash, J. Shen, S. S. Moganty, A. Corona and L. A. Archer, *Angew. Chem.-Int. Edit.*, 2011, **50**, 5904-5908.
29. F.-F. Zhang, G. Huang, X.-X. Wang, Y.-L. Qin, X.-C. Du, D.-M. Yin, F. Liang and L.-M. Wang, *Chemistry – A European Journal*, 2014, **20**, 17523-17529.
30. V. S. Kolosnitsyn, E. V. Kuzmina, E. V. Karaseva and S. E. Mochalov, *Journal of Power Sources*, 2011, **196**, 1478-1482.